Comparison of a Low Diffusion E-CUSP and the Roe Scheme for RANS Calculation

Baoyuan Wang [*], Ge-Cheng Zha[†]
Dept. of Mechanical and Aerospace Engineering
University of Miami
Coral Gables, Florida 33124
E-mail: gzha@miami.edu

Abstract

This paper is to compare the performance of recently developed low diffusion E-CUSP (LDE) scheme and Roe scheme when they are coupled with Spalart-Allmaras one equation turbulence model. The purpose is not just to understand their performance for RANS calculation. Such understanding is very useful for Detached Eddy Simulation(DES), for which the Spalart DES model is numerically based on Spalart-Allmaras one equation turbulence model. The algebraic Baldwin-Lomax turbulence model is also used as a reference to compare their numerical performance. The implicit Gauss-Seidel Line relaxation is used for time marching. For the Roe scheme, the implicit Jacobian matrix is based on the Roe scheme itself. For the LDE scheme, the implicit Jacobian is based on the Van Leer's flux vector splitting scheme. The finding of this research is: for the Baldwind-Lomax model, which does not introduce extra transport equation, both the LDE and the Roe scheme can use high CFL numbers and achieve high convergence rates; for the Spalart-Allmaras one equation turbulence model, the extra equation changes the Jacobian of the Roe scheme and weakens the diagonal dominance. It reduces the maximum CFL number permitted by the Roe scheme and hence decreases the convergence rate. The LDE scheme is only slightly affected by the extra equation and maintain high CFL number and convergence rate. Several 2D and 3D problems are calculated.

1 Introduction

Developing accurate and efficient numerical scheme remains an important issue because of the complexity of flows and geometries in practical engineering problems. The approximate Riemann solver scheme suggested by Roe [1] is widely used for compressible flow computation due to its low diffusion [2] and capability to capture the exact shock and contact discontinuities.

[*] Graduate Student, AIAA Member
[†] Associate Professor, AIAA Senior Member

However, the Roe scheme requires the calculation of the dissipation matrix, which is quite CPU time consuming. In addition, when extra equations are added such as for calculations of RANS turbulence models or chemical reaction, the eigenvalues and eigenvectors need to be re-derived, which makes the application of Roe scheme not straightforward for complicated flows.

To overcome these drawbacks, many efforts have been made to develop upwind schemes without the matrix operation for the dissipation terms. The research in this direction includes the pioneering work of the AUSM family scheme developed by Liou et al[3, 4, 5, 6], Jameson's CUSP schemes[7, 8], Edwards' low diffusion flux-splitting scheme[9, 10], and the E-CUSP schemes of Zha et al. [11, 12, 13, 14], etc.

Recently, the Detached-Eddy Simulation(DES) of turbulence proposed by Spalart[15, 16] has attracted great interest as a compromise of CPU cost and accuracy between Reynolds averaged Navier-Stokes(RANS) model and large eddy simulation (LES). Currently, many of the DES simulations rely on the Spalart-Allmaras (S-A) one equation turbulence model to calculate the eddy viscosity near the wall and the sub-grid scale stresses away from the wall[17, 18, 19, 20, 21].

As a first step to implement the DES model, this paper investigates the numerical performance of the recently developed low diffusion E-CUSP scheme [14] and the popularly used Roe scheme when they are coupled with the Spalart-Allmaras one equation turbulence model. In this paper, it is observed that the LDE scheme is more efficient and easier to be implemented with one extra equation for the turbulence model. The LDE scheme is demonstrated to work very well for DES using the Spalart-Allmaras (S-A) one equation turbulence model with the high order weighted essentially non-oscillatory (WENO) scheme[21].

2 Governing Equations

The governing equations are the Reynolds Averaged Navier Stokes(RANS) equations coupled with the S-A one equation turbulence model[22]. In generalized coordinate system, the conservative form of the equations are given as the following:

$$\frac{\partial Q}{\partial t}+\frac{\partial \mathbf{E}}{\partial \xi}+\frac{\partial \mathbf{F}}{\partial \eta}+\frac{\partial \mathbf{G}}{\partial \zeta}=\frac{1}{Re}\left(\frac{\partial \mathbf{R}}{\partial \xi}+\frac{\partial \mathbf{S}}{\partial \eta}+\frac{\partial \mathbf{T}}{\partial \zeta}+\mathbf{D}\right) \tag{1}$$

where,

$$Q=\frac{1}{J}\begin{bmatrix}\rho\\ \rho u\\ \rho v\\ \rho w\\ \rho e\\ \rho\tilde{\nu}\end{bmatrix} \tag{2}$$

$$\mathbf{E}=\begin{bmatrix}\rho U\\ \rho uU+l_x p\\ \rho vU+l_y p\\ \rho wU+l_z p\\ (\rho e+p)U-l_t p\\ \rho\tilde{\nu}U\end{bmatrix},\ \mathbf{F}=\begin{bmatrix}\rho V\\ \rho uV+m_x p\\ \rho vV+m_y p\\ \rho wV+m_z p\\ (\rho e+p)V-m_t p\\ \rho\tilde{\nu}V\end{bmatrix},\ \mathbf{G}=\begin{bmatrix}\rho W\\ \rho uW+n_x p\\ \rho vW+n_y p\\ \rho wW+n_z p\\ (\rho e+p)W-n_t p\\ \rho\tilde{\nu}W\end{bmatrix} \tag{3}$$

$$\mathbf{R}=\begin{bmatrix} 0 \\ l_k\tau_{xk} \\ l_k\tau_{yk} \\ l_k\tau_{zk} \\ l_k\beta_k \\ \frac{\rho}{\sigma}\left(\nu+\tilde{\nu}\right)\left(\mathbf{l}\bullet\nabla\tilde{\nu}\right) \end{bmatrix},\ \mathbf{S}=\begin{bmatrix} 0 \\ m_k\tau_{xk} \\ m_k\tau_{yk} \\ m_k\tau_{zk} \\ m_k\beta_k \\ \frac{\rho}{\sigma}\left(\nu+\tilde{\nu}\right)\left(\mathbf{m}\bullet\nabla\tilde{\nu}\right) \end{bmatrix},\ \mathbf{T}=\begin{bmatrix} 0 \\ n_k\tau_{xk} \\ n_k\tau_{yk} \\ n_k\tau_{zk} \\ n_k\beta_k \\ \frac{\rho}{\sigma}\left(\nu+\tilde{\nu}\right)\left(\mathbf{n}\bullet\nabla\tilde{\nu}\right) \end{bmatrix} \tag{4}$$

$$D=\frac{1}{J}\begin{bmatrix} 0 \\ 0 \\ 0 \\ 0 \\ 0 \\ S_\nu \end{bmatrix} \tag{5}$$

where

$$\beta_k=u_i\tau_{ki}-q_k \tag{6}$$

$$\begin{aligned} S_\nu=&\rho C_{b1}\left(1-f_{t2}\right)\tilde{S}\tilde{\nu}+\tfrac{1}{Re}\left[-\rho\left(C_{w1}f_w-\tfrac{C_{b1}}{\kappa^2}f_{t2}\right)\left(\tfrac{\tilde{\nu}}{d}\right)^2\right.\\ &\left.+\tfrac{\rho}{\sigma}C_{b2}\left(\nabla\tilde{\nu}\right)^2-\tfrac{1}{\sigma}\left(\nu+\tilde{\nu}\right)\nabla\tilde{\nu}\bullet\nabla\rho\right]+Re\left[\rho f_{t1}\left(\Delta U\right)^2\right] \end{aligned} \tag{7}$$

In the equations above, U, V and W are the contravariant velocities in ξ, η and ζ directions.

$$\begin{aligned} U&=l_t+\mathbf{l}\bullet\mathbf{V}=l_t+l_xu+l_yv+l_zw\\ V&=m_t+\mathbf{m}\bullet\mathbf{V}=m_t+m_xu+m_yv+m_zw\\ W&=n_t+\mathbf{n}\bullet\mathbf{V}=n_t+n_xu+n_yv+n_zw \end{aligned} \tag{8}$$

where $\mathbf{V}=(u,v,w)$ is the velocity vector, $\mathbf{l}$, $\mathbf{m}$, $\mathbf{n}$ are the normal vectors on ξ,η,ζ surfaces with their magnitudes equal to the elemental surface area and pointing to the directions of increasing ξ,η,ζ.

$$\mathbf{l}=\frac{\nabla\xi}{J}\mathrm{d}\eta\mathrm{d}\zeta,\ \mathbf{m}=\frac{\nabla\eta}{J}\mathrm{d}\xi\mathrm{d}\zeta,\ \mathbf{n}=\frac{\nabla\zeta}{J}\mathrm{d}\xi\mathrm{d}\eta \tag{9}$$

l_t, m_t, n_t stand for the grid moving velocities and are defined as

$$l_t=\frac{\xi_t}{J}\mathrm{d}\eta\mathrm{d}\zeta,\ m_t=\frac{\eta_t}{J}\mathrm{d}\xi\mathrm{d}\zeta,\ n_t=\frac{\zeta_t}{J}\mathrm{d}\xi\mathrm{d}\eta \tag{10}$$

When the grid is stationary, $l_t=m_t=z_t=0$.

Since $\Delta\xi=\Delta\eta=\Delta\zeta=1$ in the current discretization, Eqs.(9) and (10) are written as the following in the solver,

$$\mathbf{l}=\frac{\nabla\xi}{J},\ \mathbf{m}=\frac{\nabla\eta}{J},\ \mathbf{n}=\frac{\nabla\zeta}{J} \tag{11}$$

$$l_t=\frac{\xi_t}{J},\ m_t=\frac{\eta_t}{J},\ n_t=\frac{\zeta_t}{J} \tag{12}$$

The shear-stress τ_{ik} and total heat flux q_k in Cartesian Coordinate can be expressed as

$$\tau_{ik} = (\mu + \mu_t)\left[\left(\frac{\partial u_i}{\partial x_k} + \frac{\partial u_k}{\partial x_i}\right) - \frac{2}{3}\delta_{ik}\frac{\partial u_j}{\partial x_j}\right] \tag{13}$$

$$q_k = -\left(\frac{\mu}{Pr} + \frac{\mu_t}{Pr_t}\right)\frac{\partial T}{\partial x_k} \tag{14}$$

where, Pr is the Prandtl number, Pr_t is the turbulent Prandtl number, μ is the molecular viscosity determined by Sutherland law and μ_t is the turbulent viscosity determined by S-A model,

$$\mu_t = \rho\tilde{\nu}f_{v1} \tag{15}$$

The kinematic viscosity ν is defined as

$$\nu = \frac{\mu}{\rho} \tag{16}$$

In eqs.(4), (6), (13) and (14), the repeated subscripts i or k represent the coordinates x, y and z following Einstein summation convention. Eqs.(13) and (14) are transformed to generalized coordinate system in computation.

The sixth equation of the governing equations (1)-(5) is the S-A one equation turbulence model[22]. The functions in the equation are given as

$$\begin{array}{l} f_{v1} = \frac{\chi^3}{\chi^3+C_{\nu1}^3},\ \chi = \frac{\tilde{\nu}}{\nu} \\ \tilde{S} = S + \frac{\tilde{\nu}}{Re\kappa^2 d^2}f_{v2},\ f_{v2} = 1 - \frac{\chi}{1+\chi f_{v1}} \\ f_w = g\left[\frac{1+C_{w3}^6}{g^6+C_{w3}^6}\right]^{\frac{1}{6}},\ g = r + C_{w2}\left(r^6 - r\right),\ r = \frac{\tilde{\nu}}{Re\tilde{S}\kappa^2 d^2} \\ f_{t1} = C_{t1}g_t exp\left[-C_{t2}\frac{\omega_t^2}{\Delta U^2}\left(d^2 + g_t^2 d_t^2\right)\right],\ g_t = min\left(0.1, \frac{\Delta U}{\omega_t \Delta x_t}\right) \\ f_{t2} = C_{t3}exp\left(-C_{t4}\chi^2\right) \end{array} \tag{17}$$

where, $S = \sqrt{\left(\frac{\partial w}{\partial y} - \frac{\partial v}{\partial z}\right)^2 + \left(\frac{\partial u}{\partial z} - \frac{\partial w}{\partial x}\right)^2 + \left(\frac{\partial v}{\partial x} - \frac{\partial u}{\partial y}\right)^2}$ is the magnitude of vorticity which is also transformed to generalized coordinate system, ω_t is the wall vorticity at the wall boundary layer trip location, d is the distance to the closest wall. d_t is the distance of the field point to the trip location, ΔU is the difference of the velocities between the field point and the trip location, Δx_t is the grid spacing along the wall at the trip location.

The constants in S-A model are set to have the values as the following

$$\begin{array}{l} \sigma = \frac{2}{3},\ C_{b1} = 0.1355,\ C_{b2} = 0.622,\ \kappa = 0.41,\ C_{v1} = 7.1, \\ C_{w1} = C_{b1}/\kappa^2 + \left(1 + C_{b2}\right)/\sigma,\ C_{w2} = 0.3,\ C_{w3} = 2, \\ C_{t1} = 1,\ C_{t2} = 2,\ C_{t3} = 1.2,\ C_{t4} = 0.5 \end{array}$$

For large r, f_w reaches a constant. So if $r \geq 10$, we let $r = 10$.

3 The Numerical Method

The inviscid fluxes are evaluated using Van Leer's 3rd order MUSCL scheme[23] based on the LDE scheme and Roe scheme given below. The viscous term are discretized using 2nd order central differencing scheme.

3.1 The LDE Scheme [14]

The basic idea of the E-CUSP scheme is to split the inviscid flux into the convective flux E^c and the pressure flux E^p. With the one extra equation from the S-A model, the splitting is basically the same as the original scheme and is straightforward. In generalized coordinate system, the flux $\mathbf{E}$ can be split as the following

$$\mathbf{E} = E^c + E^p = \begin{pmatrix} \rho U \\ \rho u U \\ \rho v U \\ \rho w U \\ \rho e U \\ \rho \tilde{\nu} U \end{pmatrix} + \begin{pmatrix} 0 \\ l_x p \\ l_y p \\ l_z p \\ p\overline{U} \\ 0 \end{pmatrix} \tag{18}$$

where

$$\overline{U} = l_x u + l_y v + l_z w \tag{19}$$

The convective term, E^c is evaluated following the Edward's H-CUSP LDFSS [9, 10],

$$E^c = \rho U \begin{pmatrix} 1 \\ u \\ v \\ w \\ e \\ \tilde{\nu} \end{pmatrix} = \rho U f^c,\ f^c = \begin{pmatrix} 1 \\ u \\ v \\ w \\ e \\ \tilde{\nu} \end{pmatrix} \tag{20}$$

let

$$C = c\left(l_x^2 + l_y^2 + l_z^2\right)^{\frac{1}{2}} \tag{21}$$

where $c = \sqrt{\gamma RT}$ is the speed of sound. Then the convective flux at interface $\frac{1}{2}$ is evaluated as:

$$E^c_{\frac{1}{2}} = C_{\frac{1}{2}}\left[\rho_L C^+ f^c_L + \rho_R C^- f^c_R\right] \tag{22}$$

where, the subscripts L and R represent the left and right hand sides of the interface.

The interface speed of sound is

$$C_{\frac{1}{2}} = \frac{1}{2}\left(C_L + C_R\right) \tag{23}$$

The following relations borrowed from Edwards LDFFS scheme [9, 10] to express the formulations from $-\infty < M < \infty$ are used,

$$
\begin{array}{l}
C^{+} = \alpha_L^{+}\left(1+\beta_L\right)M_L - \beta_L M_L^{+} - M_{\frac{1}{2}}^{+} \\
C^{-} = \alpha_R^{-}\left(1+\beta_R\right)M_R - \beta_R M_R^{-} + M_{\frac{1}{2}}^{-} \\
M_L = \frac{U_L}{C_{\frac{1}{2}}},\ M_R = \frac{U_R}{C_{\frac{1}{2}}} \\
\alpha_{L,R} = \frac{1}{2}\left[1 \pm sign\left(M_{L,R}\right)\right] \\
\beta_{L,R} = -max\left[0, 1 - int\left(\left|M_{L,R}\right|\right)\right] \\
M_{\frac{1}{2}}^{+} = M_{\frac{1}{2}}\frac{C_R + C_L\Phi}{C_R + C_L},\ M_{\frac{1}{2}}^{-} = M_{\frac{1}{2}}\frac{C_L + C_R\Phi^{-1}}{C_R + C_L},\ \Phi = \frac{\left(\rho C^2\right)_R}{\left(\rho C^2\right)_L} \\
M_{\frac{1}{2}} = \beta_L\delta^{+}M_L^{-} - \beta_R\delta^{-}M_R^{+} \\
M_{L,R}^{\pm} = \pm\frac{1}{4}\left(M_{L,R} \pm 1\right)^2 \\
\delta^{\pm} = \frac{1}{2}\left\{1 \pm sign\left[\frac{1}{2}\left(M_L + M_R\right)\right]\right\}
\end{array}
\tag{24}
$$

The pressure flux, E^p is evaluated as the following

$$
E_{\frac{1}{2}}^{p} = \begin{pmatrix} 0 \\ p\,l_x \\ p\,l_y \\ p\,l_z \\ p\overline{U} \\ 0 \end{pmatrix} = \begin{pmatrix} 0 \\ \left(\mathcal{D}_L^{+}p_L + \mathcal{D}_R^{-}p_R\right)l_x \\ \left(\mathcal{D}_L^{+}p_L + \mathcal{D}_R^{-}p_R\right)l_y \\ \left(\mathcal{D}_L^{+}p_L + \mathcal{D}_R^{-}p_R\right)l_z \\ \overline{C}_{\frac{1}{2}}\left(\mathcal{S}_L^{+}p_L + \mathcal{S}_R^{-}p_R\right) \\ 0 \end{pmatrix} \tag{25}
$$

where,

$$
{\mathcal{D}^{\pm}}_{L,R} = \left[\alpha\left(1+\beta\right) - \beta\mathcal{P}^{\pm}\right]_{L,R} \tag{26}
$$

The pressure splitting coefficient is:

$$
\mathcal{P}_{L,R}^{\pm} = \frac{1}{4}\left(M_{L,R} \pm 1\right)^2\left(2 \mp M_{L,R}\right) \tag{27}
$$

For the pressure term in the energy equation, the contravariant speed of sound $\overline{C}$ is consistent with $\overline{U}$ and is calculated as:

$$
\overline{C} = C - l_t \tag{28}
$$

$$
{\mathcal{S}^{\pm}}_{L,R} = \left[\bar{\alpha}^{\pm}\left(1+\bar{\beta}\right)M - \bar{\beta}\bar{M}\right]_{L,R} \tag{29}
$$

where

$$
\bar{M} = \frac{\overline{U}}{\overline{\overline{C}}} \tag{30}
$$

and the $\bar{\alpha}$ and $\bar{\beta}$ are evaluated based on $\bar{M}$ using the formulations given in eq. (24). The use of $\overline{U}$, $\overline{C}$ and $\bar{M}$ in the pressure term for the energy equation is to take into account of the grid speed so

that the flux will transit from subsonic to supersonic smoothly. When the grid is stationary, $l_t = 0$, $\overline{C} = C$, $\overline{U} = U$.

The LDE scheme can accurately resolve wall boundary layer profiles, capture crisp shock profiles and exact contact surfaces [14] with low diffusion.

3.2 The Roe Scheme

Roe suggested his approximate Riemann solver in 1D form in 1981[1]. Take ξ direction as the example, the flux at interface $\frac{1}{2}$ is calculated as the following

$$E_{\frac{1}{2}} = \frac{1}{2}\left[E_L + E_R + \tilde{T}|\tilde{\Lambda}|\tilde{T}^{-1}\left(Q_L - Q_R\right)\right] \tag{31}$$

Let $A = \frac{\partial E}{\partial Q}$ be the Jacobian matrix with the extra equation of S-A model. A is a 6×6 matrix and has the form $A = T\Lambda T^{-1}$, where T is the right eigenvector matrix of A, Λ is the eigenvalue matrix of A. $\tilde{T}$ and $\tilde{\Lambda}$ have the same expression as T and Λ, but the variables are replaced by their corresponding Roe-averaged counterparts. Λ and T are given as the following

$$\Lambda = \begin{pmatrix} U+C & & & & & \\ & U-C & & 0 & & \\ & & U & & & \\ & 0 & & U & & \\ & & & & U & \\ & & & & & U \end{pmatrix} \tag{32}$$

$$T = \begin{pmatrix} \frac{1}{2h} & \frac{1}{2h} & 0 & 0 & -\frac{1}{h} & 0 \\ \frac{u+c\hat{l}_x}{2h} & \frac{u-c\hat{l}_x}{2h} & \hat{m}_x & \hat{n}_x & -\frac{u}{h} & 0 \\ \frac{v+c\hat{l}_y}{2h} & \frac{v-c\hat{l}_y}{2h} & \hat{m}_y & \hat{n}_y & -\frac{v}{h} & 0 \\ \frac{w+c\hat{l}_z}{2h} & \frac{w-c\hat{l}_z}{2h} & \hat{m}_z & \hat{n}_z & -\frac{w}{h} & 0 \\ \frac{c\hat{U}+\gamma e-(\gamma-1)\,q}{2h} & \frac{-c\hat{U}+\gamma e-(\gamma-1)\,q}{2h} & \hat{V} & \hat{W} & -\frac{q}{h} & 0 \\ \frac{\nu}{2h} & \frac{\nu}{2h} & 0 & 0 & -\frac{\nu}{h} & 1 \end{pmatrix} \tag{33}$$

where the static enthalpy h is calculated as,

$$h = \frac{c^2}{\gamma - 1} \tag{34}$$

q is the flow kinetic energy

$$q = \frac{1}{2}\left(u^2 + v^2 + w^2\right) \tag{35}$$

$\hat{\mathbf{l}}$ is the unit vector normal to ξ surface pointing to the direction that ξ increases,

$$\hat{\mathbf{l}} = \frac{\mathbf{l}}{|\mathbf{l}|} \tag{36}$$

$\hat{\mathbf{m}}, \hat{\mathbf{n}}$ and $\hat{\mathbf{l}}$ are mutually orthogonal unit vectors, that is $\hat{\mathbf{l}} \bullet \hat{\mathbf{m}} = 0$, $\hat{\mathbf{l}} \bullet \hat{\mathbf{n}} = 0$, $\hat{\mathbf{m}} \bullet \hat{\mathbf{n}} = 0$.

Let $\mathbf{V} = (u, v, w)$ be the velocity vector, $\hat{U}$, $\hat{V}$ and $\hat{W}$ are then determined by,

$$\hat{U} = \mathbf{V} \cdot \hat{\mathbf{l}} \tag{37}$$

$$\hat{V} = \mathbf{V} \cdot \hat{\mathbf{m}} \tag{38}$$

$$\hat{W} = \mathbf{V} \cdot \hat{\mathbf{n}} \tag{39}$$

To preserve the low diffusion of the Roe scheme, no entropy fix is used with the Roe scheme.

3.3 Implicit Time Integration

In the current work, the finite volume method is used to discretize the governing equations for steady state solution. To achieve high convergence rate, the implicit time marching scheme is used with the unfactored Gauss-Seidel line relaxation. To enhance diagonal dominance, the first order Euler method is used to discrete the temporal term

$$\begin{array}{l} \frac{\Delta V}{\Delta t}\left(Q^{n+1} - Q^n\right) + \left(E_{i+\frac{1}{2}} - E_{i-\frac{1}{2}}\right)^{n+1} + \left(F_{j+\frac{1}{2}} - F_{j-\frac{1}{2}}\right)^{n+1} + \left(G_{k+\frac{1}{2}} - G_{k-\frac{1}{2}}\right)^{n+1} \\ \quad = \frac{1}{Re}\left[\left(R_{i+\frac{1}{2}} - R_{i-\frac{1}{2}}\right)^{n+1} + \left(S_{j+\frac{1}{2}} - S_{j-\frac{1}{2}}\right)^{n+1} + \left(T_{k+\frac{1}{2}} - T_{k-\frac{1}{2}}\right)^{n+1} + D^n \cdot \Delta V\right] \end{array} \tag{40}$$

where n and $n+1$ are two sequential time levels with a time interval of Δt.

The first-order Taylor expansion for $n+1$ time level is used for all inviscid and viscous terms above. The discretized equations are given as the following

$$\begin{array}{l} \Delta Q^{n+1}_{i,j,k} + A^+\Delta Q^{n+1}_{i+1,j,k} + A\Delta Q^{n+1}_{i,j,k} + A^-\Delta Q^{n+1}_{i-1,j,k} + B^+\Delta Q^{n+1}_{i,j+1,k} + B\Delta Q^{n+1}_{i,j,k} \\ +B^-\Delta Q^{n+1}_{i,j-1,k} + C^+\Delta Q^{n+1}_{i,j,k+1} + C\Delta Q^{n+1}_{i,j,k} + C^-\Delta Q^{n+1}_{i,j,k-1} = RHS^n \end{array} \tag{41}$$

where RHS^n is the summation of all the terms on the right hand side (RHS) of the equation.

$$\begin{array}{rl} RHS^n = \frac{\Delta t}{Re\Delta V}\Bigg\{\Bigg[\left(R^n_{i+\frac{1}{2}} - R^n_{i-\frac{1}{2}}\right) + \left(S^n_{j+\frac{1}{2}} - S^n_{j-\frac{1}{2}}\right) + \left(T^n_{k+\frac{1}{2}} - T^n_{k-\frac{1}{2}}\right)\Bigg] \\ \quad - \Bigg[\left(E^n_{i+\frac{1}{2}} - E^n_{i-\frac{1}{2}}\right) + \left(F^n_{j+\frac{1}{2}} - F^n_{j-\frac{1}{2}}\right) + \left(G^n_{k+\frac{1}{2}} - G^n_{k-\frac{1}{2}}\right)\Bigg]\Bigg\} + \frac{1}{Re}D^n \cdot \Delta t \end{array} \tag{42}$$

The Gauss-Seidel line relaxation is applied on each direction respectively and is swept forward and backward once within each physical time. For example, if the sweeping is in i direction from smaller index to larger one, eq.(41) will be

$$B^-\Delta Q^{n+1}_{i,j-1,k} + \bar{B}\Delta Q^{n+1}_{i,j,k} + B^+\Delta Q^{n+1}_{i,j+1,k} = RHS' \tag{43}$$

where, $\bar{B} = I + A + B + C$. The terms in the neighboring cells in i and k directions are absorbed into RHS^n as RHS',

$$RHS' = RHS^n - A^+\Delta Q^n_{i+1,j,k} - A^-\Delta Q^{n+1}_{i-1,j,k} - C^+\Delta Q^n_{i,j,k+1} - C^-\Delta Q^{n+1}_{i,j,k-1} \tag{44}$$

The unfactored implicit Gauss-Seidel line relaxation employed in this paper is significantly more efficient than the LU-SGS implicit scheme[25].

3.4 Initial and Boundary Conditions for Spalart-Allmaras one equation Turbulence Model

In S-A one equation turbulence model, the trip point need to be specified before computation. This is not straightforward to do because the exact position of the trip point is not known in most of the cases. Thus, a full turbulent boundary layer is used in this paper by setting $C_{t1} = 0$ and $C_{t3} = 0$. No trip point needs to be specified

It is observed that the S-A one equation turbulence model is sensitive to initial field. If the initial field of $\tilde{\nu}$ is set to a small value, e.g. $\tilde{\nu} < 1$, the solution may converge with $\tilde{\nu} = 0$, which is the trivial solution of $\tilde{\nu}$ when $C_{t1} = C_{t3} = 0$. This will result in a laminar flow solution. If the initial value is too large ($\tilde{\nu} > 3$), the computation may diverge. In addition, setting up the initial value of $\tilde{\nu}$ also depends on the schemes to be used. For example, if the initial value of $\tilde{\nu}$ is set to 1, the LDE scheme converges to a correct answer. However, for the subsonic flat plate turbulent boundary layer flow and RAE2822 airfoil, the Roe scheme will converge to a laminar flow solution. In our computation, it is found that it is generally safe to set the initial value of $\tilde{\nu}$ to 2.

The boundary conditions of $\tilde{\nu}$ are given as the following

$$\begin{array}{ll} at\ walls: & \tilde{\nu} = 0 \\ far\ field\ inflow: & \tilde{\nu} = 0.02 \\ far\ field\ outflow: & \tilde{\nu}\ is\ extrapolated \end{array}$$

4 Results and Discussion

Several 2D and 3D cases have been computed using the LDE scheme and the Roe scheme to compare their performance. Both S-A one equation model and B-L algebraic model are used for the computation.

4.1 Subsonic Flat Plate Turbulent Boundary Layer Flow

The subsonic flat plate is used to examine the performance of the LDE scheme for turbulent boundary layer. The mesh size is 80×60. The y^+ of the first cell center to the wall is kept less then 1.0. The Reynolds number is 4×10^6 based on the length of the plate. The inlet Mach number is 0.5.

As shown in Fig. 1, both the computational results of LDE scheme and the Roe scheme agree well with the law of the wall using S-A model. They are slightly better than the results using B-L model in the transition region from the linear viscous sublayer to log layer. With the B-L model, both schemes can use a large CFL number(≥ 100). With the S-A model, the CFL number can be

set to 100 for LDE scheme. But for Roe scheme, it can be only set to about 10. That means the Roe scheme needs more time steps to converge a result than the LDE scheme and hence, need more computational time. Fig. 2 shows the solution residuals of the LDE scheme and the Roe scheme for S-A and B-L turbulence model. The LDE scheme only use about $\frac{1}{5}$ of the CPU time required by the Roe scheme.

4.2 RAE2822 Transonic Airfoil

The RAE2822 transonic airfoil is used to compare the performance of the LDE and Roe scheme with S-A model for computing 2D turbulent transonic flows. The mesh is a two-block O-grid with dimensions of $2 \times (129 \times 56)$ as shown in Fig. 3. The Reynolds number is 6.5×10^6 based on the chord length. The Mach number is 0.729. The angle of attack is 2.31°.

Fig. 4 shows the convergence histories of the LDE scheme and the Roe scheme. The maximum CFL number that the Roe scheme can use is 6.0, whereas the LDE scheme can use 10. The LDE scheme achieves significantly faster convergence rate and lower residual level. Fig. 5 presents the comparison of pressure coefficients between the experimental data and computation results. The results of the LDE scheme and Roe scheme are virtually identical and the predicted shock locations agree well with the experiment.

4.3 Transonic Inlet-Diffuser

The transonic inlet-diffuser is used to examine the performance of the LDE scheme for shock wave/turbulent boundary layer interaction. The mesh is a single-block, 2D H-grid with dimension of 193×97 (Fig. 6). The Reynolds number is 4.38×10^5 based on the throat height. The inlet Mach number is 0.5. The exit back pressure equals to 0.72 times of the inlet total pressure.

Fig. 7 presents the comparison of the experimental data and the computational results. It shows that, with the S-A model, the LDE scheme and Roe scheme have nearly identical results. The S-A model predicts the results significantly better than the B-L model. Fig. 8 is the Mach contours of the LDE scheme, which indicates that the upper wall boundary layer is separated due to the shock/boundary layer interaction. This case shows that the turbulence model is a critical factor for the prediction accuracy of the shock wave/turbulent boundary layer interaction.

4.4 Transonic ONERA M6 Wing

The transonic ONERA M6 wing is calculated to examine the performance of the LDE scheme for three dimensional cases. The mesh is a two blocks, O-grid with the dimensions of $2 \times (72 \times 60 \times 40)$(Fig. 9). The Mach number is 0.8395. The Reynolds number is 1.97×10^7. The angle of attack is 0°.

Fig. 10 presents the comparison of the pressure distribution between the experiment and computation at the different sections. The location of $z/b = 0.2$ is near the root and $z/b = 0.99$ is near the tip of the wing. The computation results agree well with the experimental data except at the section of z/b=0.8, where the double-shock pattern is not well resolved as most of other CFD simulations.

4.5 3D Transonic Channel Flow

The 3D transonic channel flow is used to examine the performance of the LDE scheme and the Roe scheme for 3D shock wave/turbulent boundary layer interaction problems with S-A model. A single H-grid with the dimensions of $90 \times 60 \times 60$ is used in the computation(Fig. 11). The Reynolds number is 10^6 based on the entrance height. For boundary conditions, the total pressure, total temperature and flow angle are fixed at the inlet and the static pressure at the outlet is adjusted to match the position of the shock wave obtained by the experiment.

Fig. 12 to Fig. 14 present the comparison of the Mach number contours between experiment and computation at three spanwise sections. The computed shock wave structures of LDE scheme and the Roe scheme agree well with each other and are similar to that of the experiment. At the two locations close to the side wall at $z = 60mm$ and $z = 90mm$, both the computations over predict the size of separation zone. At the mid section $z = 70mm$, the predicted separation size and pattern agree well with the experiment.

5 Conclusions

A low-diffusion E-CUSP (LDE) scheme coupled with Spalart-Allmaras one equation turbulence model has been examined by 2D and 3D problems. Since LDE scheme has no matrix operation and the allowable CFL number is larger than that of the Roe scheme, the computational efficiency is significantly higher.

For the subsonic flat plate turbulent boundary layer flow, both the LDE and the Roe scheme have obtained basically identical results and all agree well with the law of the wall. However, the CPU time of the LDE scheme is only about 1/5 of the Roe scheme. For the RAE2822 airfoil, both the results using the LDE and the Roe scheme agree well with the experiment. Again, the LDE scheme achieves significantly better convergence rate and less CPU time with the L2-Norm residual converged to lower level. For the 2D inlet diffuser, the results with S-A model are significantly better than the results with B-L model. Both the schemes give the results in good agreement with the measured results of the shock wave/turbulent boundary layer interaction. For the 3D transonic ONERA M6 wing, the computational results also agree well with the experiment. For the 3D transonic channel flow, the computed shock wave structure using LDE scheme is nearly the same as that using the Roe scheme and is similar to the experiment. In the middle section, the predicted separation behind the throat using both the LDE and Roe scheme agree well with the experiment. In the section near the wall, the predicted separation zone is larger than the measured separation one.

In conclusion, the LDE scheme coupled with S-A one equation turbulence model is shown to be accurate, efficient and robust for 2D and 3D transonic viscous flow computation.

6 Acknowledgment

This work is partially supported by AFOSR Grant FA9550-06-1-0198 monitored by Fariba Fahroo.

References

[1] P. Roe, "Approximate Riemann Solvers, Parameter Vectors, and Difference Schemes," *Journal of Computational Physics*, vol. 43, pp. 357–372, 1981.

[2] B. Van Leer, J. Thomas, P. L. Roe, and R. Newsome, "A Comparison of Numerical Flux Formulas for the Euler and Navier-Stokes Equations." AIAA paper 87-1104, 1987.

[3] M.-S. Liou and C. J. Steffen, "A New Flux Splitting Scheme," *Journal of Computational Physics*, vol. 107, pp. 1–23, 1993.

[4] M.-S. Liou, "Progress Towards an Improved CFD Methods: AUSM$^+$." AIAA Paper 95-1701-CP, June, 1995.

[5] M.-S. Liou, "A Sequel to AUSM: AUSM$^+$," *Journal of Computational Physics*, vol. 129, pp. 364–382, 1996.

[6] M.-S. Liou, "Ten Years in the Making-AUSM-Family." AIAA 2001-2521, 2001.

[7] A. Jameson, "Analysis and Design of Numerical Schemes for Gas Dynamics I: Artificial Diffusion, Upwind Biasing, Limiters and Their Effect on Accuracy and Multigrid Convergence in Transonic and Hypersonic Flow," *Journal of Computational Fluid Dynamics*, vol. 4, pp. 171–218, 1995.

[8] A. Jameson, "Analysis and Design of Numerical Schemes for Gas Dynamics II: Artificial Diffusion and Discrete Shock Structure," *Journal of Computational Fluid Dynamics*, vol. 5, pp. 1–38, 1995.

[9] J. R. Edwards, "A Low-Diffusion Flux-Splitting Scheme for Navier-Stokes Calculations." AIAA Paper 95-1703-CP, June, 1995.

[10] J. R. Edwards, "A Low-Diffusion Flux-Splitting Scheme for Navier-Stokes Calculations," *Computer & Fluids*, vol. 6, pp. 635–659, 1997.

[11] G.-C. Zha and E. Bilgen, "Numerical Solutions of Euler Equations by Using a New Flux Vector Splitting Scheme ," *International Journal for Numerical Methods in Fluids*, vol. 17, pp. 115–144, 1993.

[12] G.-C. Zha and Z.-J. Hu, "Calculation of Transonic Internal Flows Using an Efficient High Resolution Upwind Scheme," *AIAA Journal*, vol. 42, No. 2, pp. 205–214, 2004.

[13] G.-C. Zha, "Low Diffusion Efficient Upwind Scheme ," *AIAA Journal*, vol. 43, 2005.

[14] G.-C. Zha, Y. Shen, and B. Wang, "Calculation of Transonic Flows Using WENO Method with a Low Diffusion E-CUSP Upwind Scheme." AIAA Paper 2008-0745, 46th AIAA Aerospace Sciences Meeting, Reno, NV, Jan. 2008.

[15] P. Spalart, W.-H. Jou, M. Strelets, and S. Allmaras, "Comments on the Feasibility of LES for Wings, and on a Hybrid RANS/LES Approach." Advances in DNS/LES, 1st AFOSR Int. Conf. on DNS/LES, Greyden Press, Columbus, H., Aug. 4-8, 1997.

[16] P. R. Spalart, "Young-Person's Guide to Detached-Eddy Simulation Grids." NASA/CR-2001-211032, 2001.

[17] A. Tarvin, M. Shur, M. Strelets, and P. Spalart, "Detached-Eddy Simulations Past a Circular Cylinder," *Flow Turbulence and Combustion*, vol. 63, 1999.

[18] A. Viswanathan, K. Klismith, J. Forsythe, and K. D. Squires, "Detached-Eddy Simulation around a Forebody at High Angle of Attack." AIAA-2003-0263, 2003.

[19] R. P. Hansen and J. Forsythe, "Large and Detached Eddy Simulation of a Circular Cylinder Using Unstructured Grids." AIAA-2003-0775, 2003.

[20] J. R. Forsythe, K. A. Hoffmann, and K. D. Cummings, R. M. Squires, "Detached-Eddy Simulations with Compressibility Corrections Applied to Supersonic Axisymmetric Base Flow," *Journal of Fluids Engineering*, vol. 124, 2002.

[21] B. Wang, G.-C. Zha, and Y. Shen, "Detached Eddy Simulations of a Circular Cylinder Using a Low Diffusion E-CUSP and High-Order WENO Scheme." submitted to 38th AIAA Fluid Dynamics Conference, Seattle, Washington, June 2008.

[22] P. Spalart and S. Allmaras, "A One-equation Turbulence Model for Aerodynamic Flows." AIAA-92-0439, 1992.

[23] B. Van Leer, "Towards the Ultimate Conservative Difference Scheme, III," *Journal of Computational Physics*, vol. 23, pp. 263–75, 1977.

[24] B. Van Leer, "Flux-Vvector Splitting for the Euler Equations," *Lecture Note in Physics*, vol. 170, pp. 507–512, 1982.

[25] Y.-Q. Shen and G.-C. Zha, "AComparison Study of Gauss-Seidel Iteration Methods for Internal and External Flows ." AIAA Paper 2007-4332, 2007.

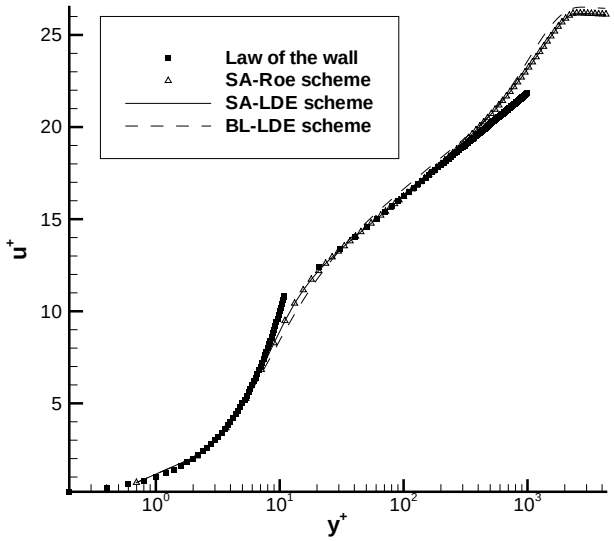

Figure 1: Comparison of velocity profiles

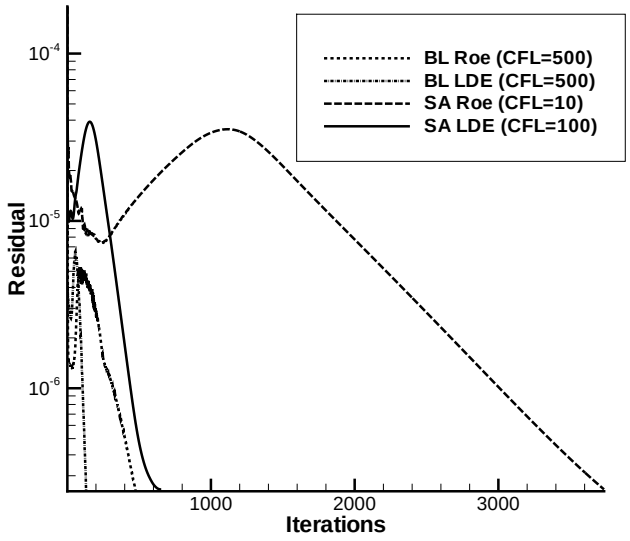

Figure 2: The L2 solution residual history of flat plate

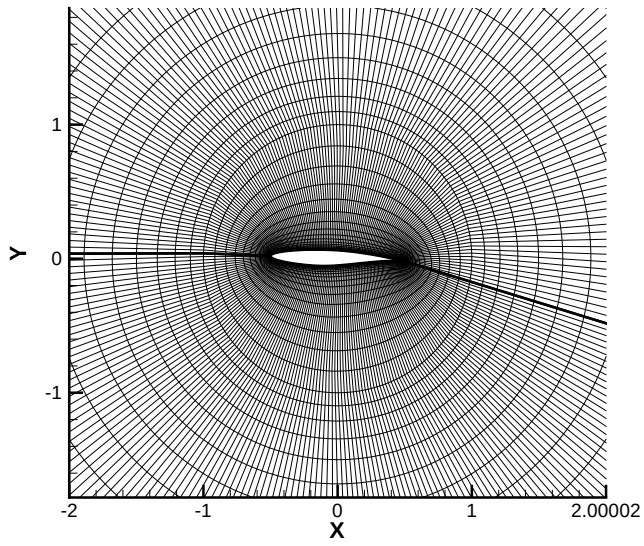

Figure 3: 2-Block grids for RAE2822

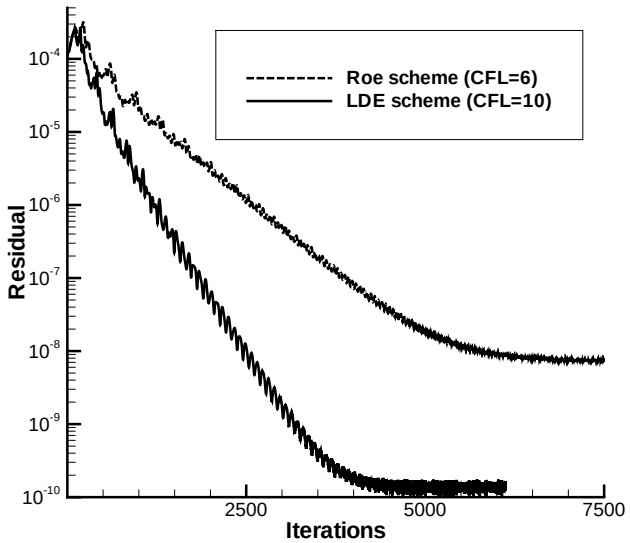

Figure 4: The L2 solution residual history of RAE2822

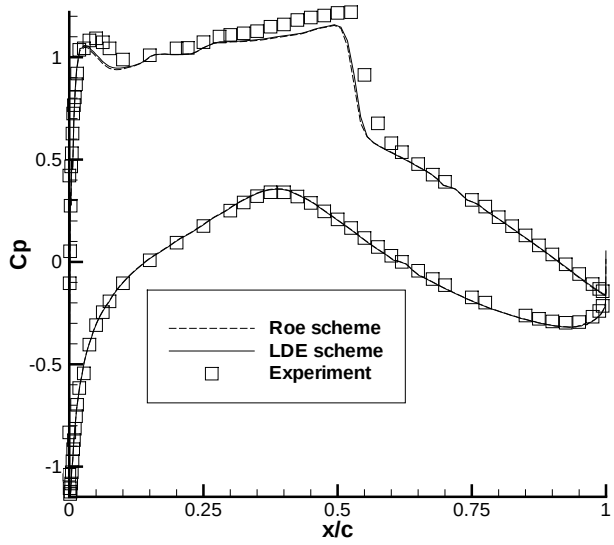

Figure 5: The surface pressure coefficient distribution of RAE2822

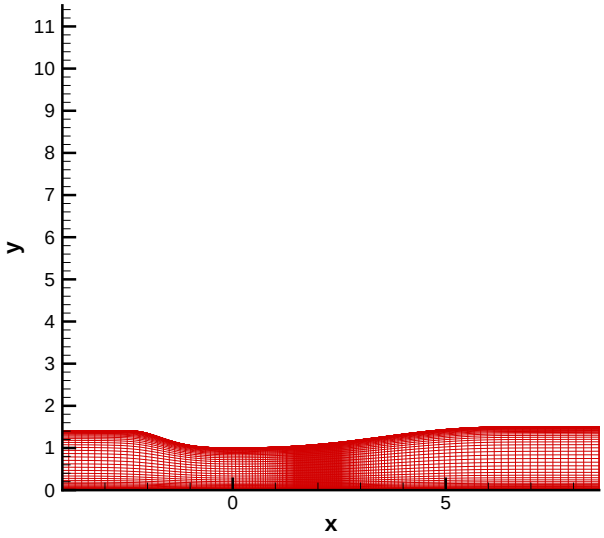

Figure 6: The mesh for 2D Inlet diffuser

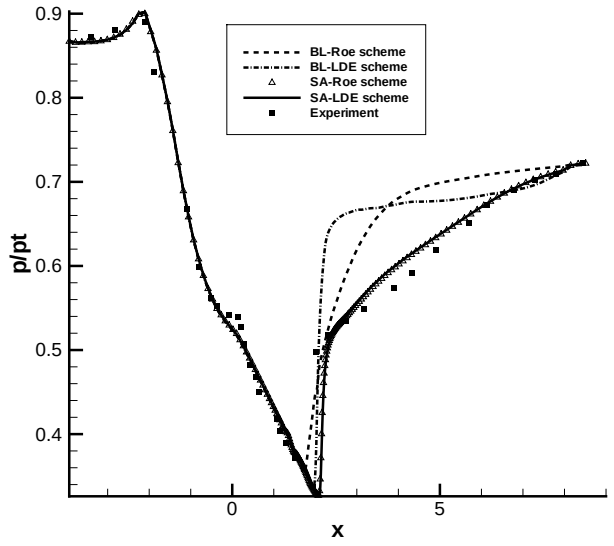

Figure 7: Upper wall pressure distribution of the inlet diffuser

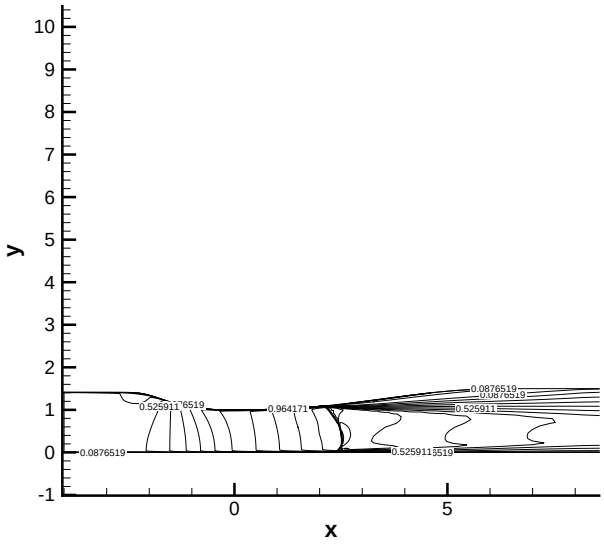

Figure 8: The contours of the Mach number for inlet diffuser

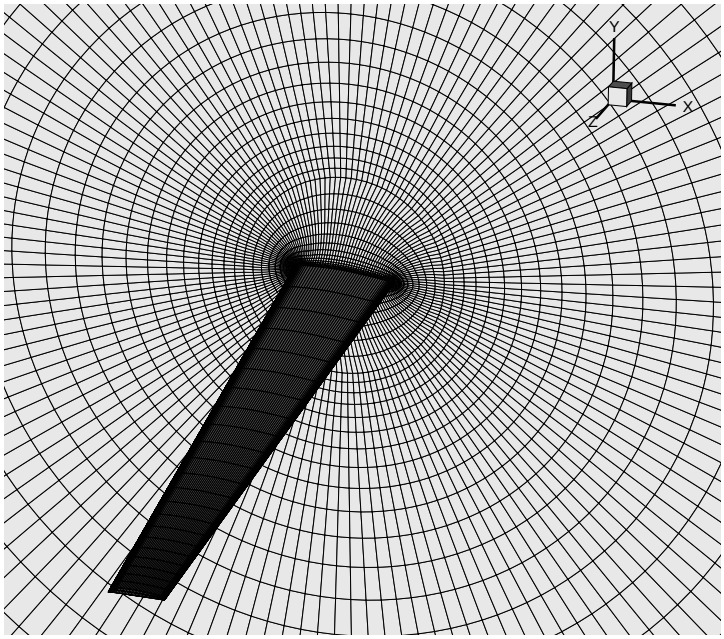

Figure 9: M6 wing mesh

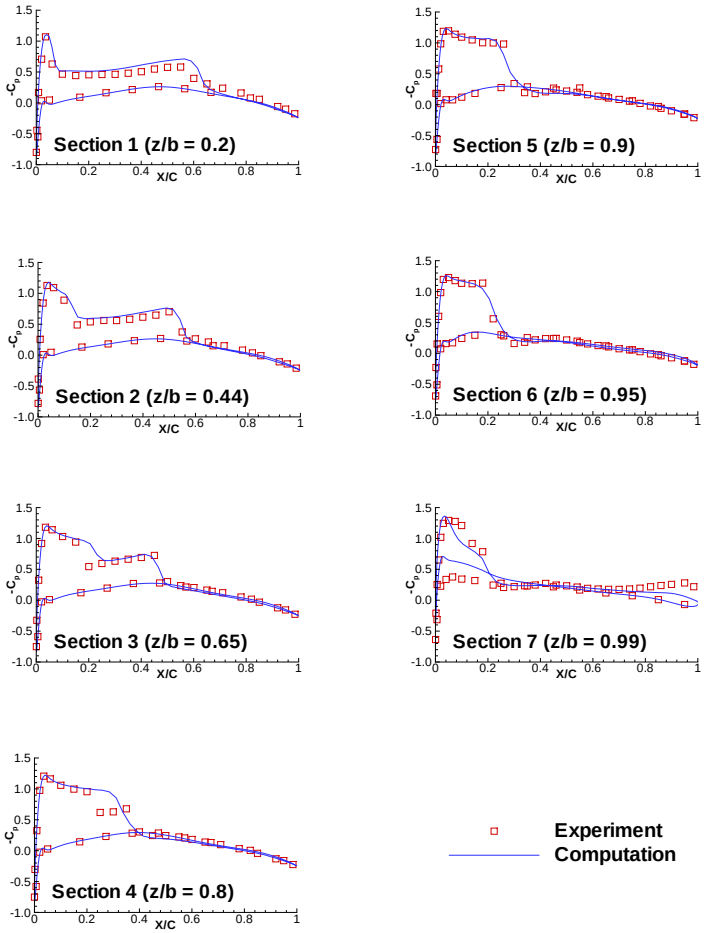

Figure 10: The surface pressure coefficient distribution of M6 wing

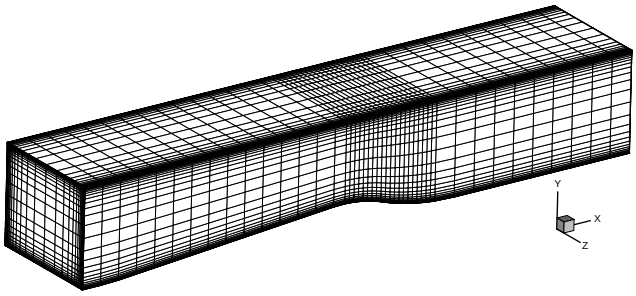

Figure 11: Transonic duct 3D mesh

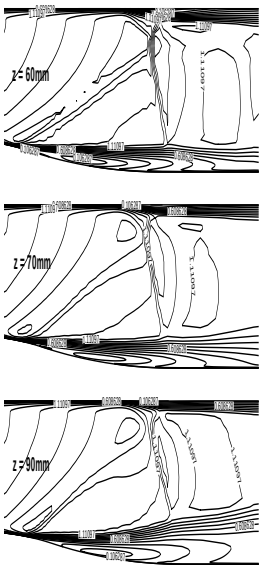

Figure 12: LDE scheme

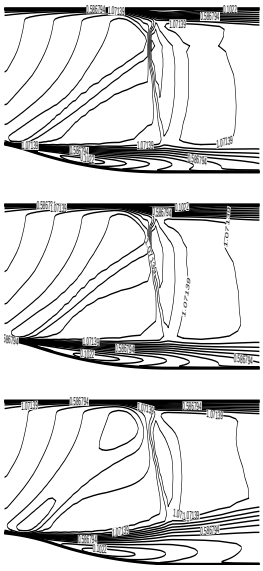

Figure 13: Roe scheme

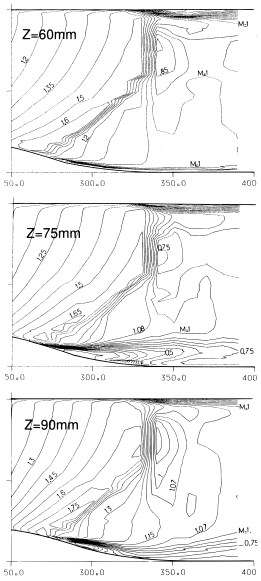

Figure 14: Experiment